SLAC-PUB-8212
October, 2000

Secondary Electron Emission Yields From PEP-II Accelerator Materials†

R. E. KIRBY and F. K. KING, *Stanford Linear Accelerator Center*
Stanford University, Stanford, CA 94309

±*Abstract*

The PEP-II B-Factory at SLAC operates with aluminum alloy and copper vacuum chambers, having design positron and electron beam currents of 2 and 1 A, respectively. Titanium nitride coating of the aluminum vacuum chamber in the arcs of the positron ring is needed in order to reduce undesirable electron-cloud effects. The total secondary electron emission yield of TiN-coated aluminum alloy has been measured after samples of beam chamber material were exposed to air and again after electron-beam bombardment, as a function of incident electron beam angle and energy. The results may be used to simulate and better understand electron-cloud effects under actual operating conditions. We also present yield measurements for other accelerator materials because new surface effects are expected to arise as beam currents increase. Copper, in particular, is growing in popularity for its good thermal conductivity and self-radiation-shielding properties. The effect of electron bombardment, "conditioning", on the yield of TiN and copper is shown.

1 Introduction

A fast multibunch instability, first observed at the Photon Factory [1], was later attributed [2] to the formation of trapped "electron clouds." The primary origin of an electron cloud accompanying a positively-charged beam is the synchrotron radiation from the beam leading to photoelectric production at the vacuum chamber walls. In addition, as the electrons "rattle around" the chamber under the influence of the beam, secondary emission from the vacuum chamber walls can seriously compound the effect. This is particularly true for the case of clean aluminum, whose native oxide surface layer has a secondary emission yield (SEY) peak value typically in the range 2-3.

The PEP-II low energy positron ring (LER) will have, at full luminosity, a stored current of 2 A with aluminum alloy vacuum chambers in the arcs, conditions which might be expected to lead to an electron cloud effect. As a result, a SEY-lowering coating has been applied to the aluminum vacuum chamber walls. TiN was sputter-deposited onto the walls to a typical thickness of 100 nm. TiN has been used routinely at SLAC [3] for the suppression of secondary electrons in s-band accelerating structures, for example, on storage ring rf tuners, and on other components with high surface electric fields. The SEY dependence on the surface chemical behavior of TiN had been previously investigated [4] by x-ray photoelectron spectroscopy (XPS), after deposition and after exposure to air. However, aluminum substrates were not used in that study and the SEY data was for perpendicular primary electron beam incidence only.

In the current study, we present SEY data for angles of primary electron incidence from normal to near-grazing for TiN-coated aluminum alloy extrusion material. Such data can be used as inputs to simulation studies whose aim is to improve understanding of the dynamics of the positron beam under the effects of the electron cloud. Important to such models is the behavior of the SEY as a function of both primary electron energy and incidence angle. Although the principal focus of this report is on the relationship between the electron cloud effect and suppressing the high SEY of uncoated aluminum alloy, other materials are used in accelerating structures and are expected to show new beam-surface interactions in future. We address this by presenting SEY results for OFE copper and type 304 stainless steel. Extruded OFE copper was used to fabricate the PEP-II high energy ring (HER) chambers, so chosen to dissipate a synchrotron radiation linear thermal flux of 100 W/cm as well as to provide low rf impedance, low gas photodesorption yield and radiation self-shielding. Measurements of angular SEY, similar to those for the LER chamber material, were also made for the HER material and for polished copper. Polished copper is of interest for w-band rf structures where the characteristic beam accelerating cavity length is a few millimeters and surface roughness and tolerancing are sub-micron.

2 Experimental Details

The TiN-coated ASTM type 6063 aluminum (99 weight per cent) alloy coupons were sectioned from a LER chamber. The surface finish is shown in Figure 1, in an atomic force micrograph. There is a strongly textured chamber extrusion orientation, which required that SEY grazing angle measurements be done both parallel and

†Work supported by the U.S. Department of Energy under contract number DE-AC03-76SF00515.

Submitted to Nuclear Instruments & Methods in Physics Research A

perpendicular to the texture (the grooves are parallel to the circulating positron beam).

The chamber coating method was discussed previously in detail [5] and consists of DC nitrogen ion-reactive sputtering from an axial Ti cathode placed in the beam chamber. Witness coupons were mounted in the chamber beam-position-monitor ports at a distance of 1.5 cm from

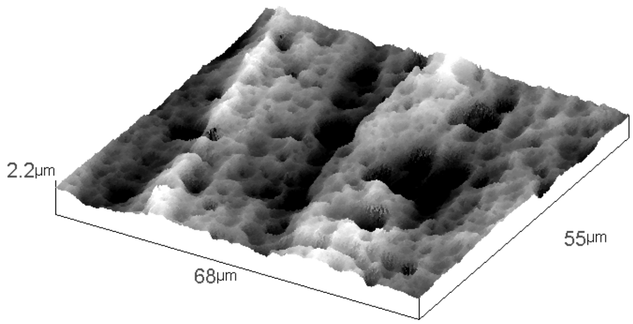

Figure 1. Surface texture of alkali-cleaned LER chamber material for PEP-II, uncoated. Etch pits are evident. RMS roughness = 0.3 µm.

the cathode. The coating color was generally black for the thickest layers. This was due to the porous nature of the deposited film [6], which also absorbed water upon exposure to air. Rutherford backscattering spectrometry confirmed that the film contained ~ 25 atomic per cent oxygen, probably from the absorbed water. However, the TiN film stoichiometry, as measured by XPS, gave Ti/N ratios consistently in the 0.9-1.1 range. Coating thicknesses were typically 100±20nm, measured by low-energy x-ray fluorescence [7], after deposition and coupon removal from the beam chambers.

HER copper was sectioned from a chamber and cleaned using the PEP-II recipe [8]. The as-extruded surface texture was much finer than that of the LER and was completely removed by the cleaning process. Other materials analyzed were: 1) uncoated LER aluminum alloy, 2) mechanically mirror-polished (0.25 micron diamond) and degreased OFE copper and, 3) chemically-etched and passivated ASTM type 304 stainless steel. In addition, every SEY measurement data set was preceded by a measurement on graphitic carbon, to confirm proper equipment operation.

SEY measurements were made by two methods, the first of which is used for perpendicular primary beam incidence only, the so-called "retarding potential" (RP) method, shown in Figure 2. The RP method has several important advantages for use in a multi-technique surface analysis system. Commercial electron guns used for surface analysis are not current-controlled at the very low level of beam currents used for yield measurements (typically a few nanoamps, to reduce beam exposure-induced effects). Also, these guns reach a space-charge limit at a cathode potential of 300-500 V. The RP technique allows fixing of the gun cathode at moderately high potential (1-2 kV), with thermal stabilization of the beam current accomplished by voltage-control of the filament emission. Then the incident primary electron energy is easily changed by sample retardation, without affecting the beam current. A second advantage is that, after the application of -10 or -20 V retarding potential to the sample, secondaries generated from nearby surfaces by elastically reflected primaries cannot be collected by the sample. The disadvantage of the RP method is that measurements are possible only at normal incidence, because the "retarding" field becomes a "deflecting" field for off-normal incidence and moves the beam from the point of measurement on the sample. For normal incidence, the SEY was measured by RP from 50 to 1100 eV primary energy, at very low beam current (electron dose/yield curve ≈2 x 10^{15} cm^{-2}) to minimize surface modification effects.

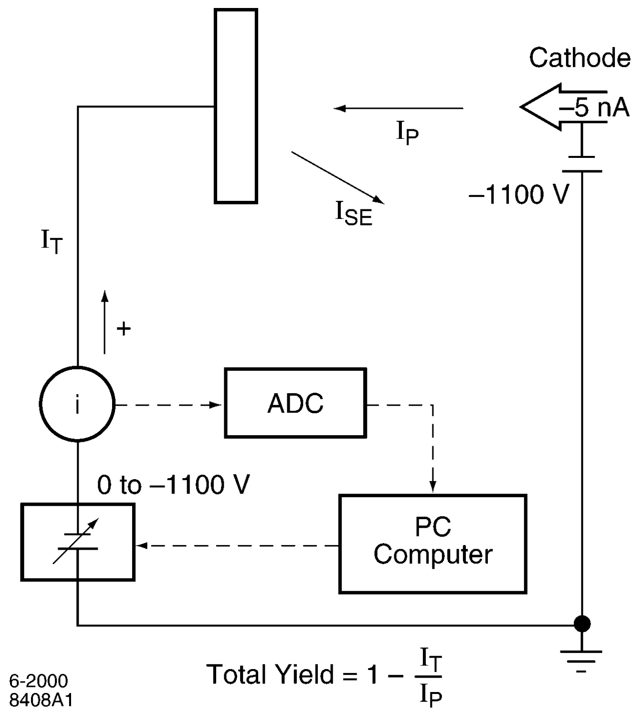

Figure 2. Circuit for retarding potential yield measurements, perpendicular incidence electron beam.

The SEY angular measurements (Figure 3) were made by stepwise reducing the energy of the gun (zero retard, ZR, method) with the sample grounded, until the space charge limit of the gun was reached at 300 eV (the principal disadvantage to this method). In this mode, the electron gun current changes as a function of electron accelerating potential. After allowing the gun to reach thermal equilibrium, the beam current was measured to a positively-biased carbon collector and was found to remain consistently repeatable during the course of a measurement series. The angular incidence of the primary electron beam is referenced to the sample surface normal, i.e., 0^o is normal incidence.

Contributions to the sample current from electron backscatter-bombardment of nearby surfaces (all graphite-coated) were measured at normal incidence using both RP and ZR methods. Secondaries generated at these surfaces have mostly very low energy and serve to strike and reduce the apparent yield of the sample. ZR curves need to be corrected (< 5%) for this effect. Primary electrons elastically scattering in the forward direction from the surface at grazing incidence were collected in a "black-hole" gridded structure behind the sample holder. The sample was moved laterally several electron beam diameters between successive angular measurements, to ensure that a previously-unbombarded area was used for the next SEY measurement.

XPS measurements were made on TiN-coated samples in a separate UHV system and then the samples were transferred to the SEY-measurement chamber. The SEY-measurement chamber has an Auger electron spectrometer (AES), which is used to check surface chemistry on a spot several mm away from the SEY-measurement area. Conditions in this system are similar to the LER, cleaned for UHV operation and unbaked with a pressure of one ntorr or so.

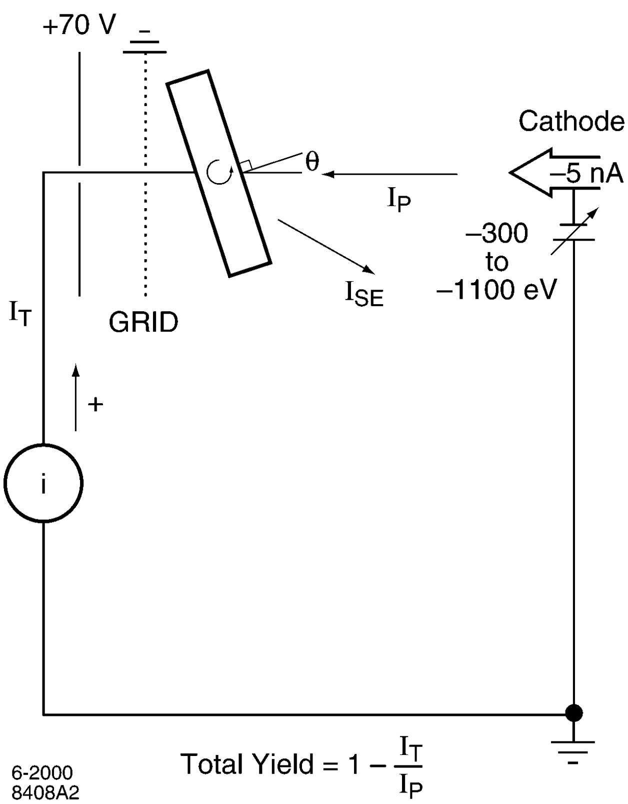

Figure 3. Circuit for zero retard yield measurements, angular beam incidence. The volume around the sample is at ground potential and field-free.

3. Results

3.1 General Comments

Figure 4 shows the unacceptably large (for beam chamber use) peak SEY of >2 of air-oxidized etched aluminum alloy. In fact, chemically removing residual carbon from the surface serves to increase the SEY by increasing the percentage of surface covered by high-yield aluminum oxide in place of lower yield carbon. Copper has a much lower yield and need not, for present machines at least, be coated with a SEY-lowering material. For aluminum alloy chambers and high-field components, TiN coating is frequently used. However, chambers are always exposed

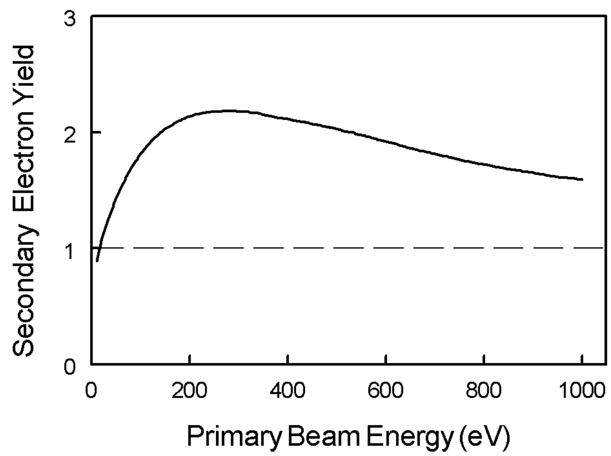

Figure 4. SEY of alkali-etched Al alloy in Figure 1.

to atmosphere following coating, which leads to a rise in the SEY of the coated surface. Such surfaces need to be "conditioned" in situ to restore a low SEY.

Conditioning of beam chambers, i.e., an in-situ reduction of the gas load from the chamber walls occurs by synchrotron light and electron bombardment. This process and its effect on the SEY of the walls is characterized as follows. The as-deposited/air-exposed SEY (e.g., TiN-coated aluminum alloy, Figure 5, inset) is mainly determined by the presence of a surface water and hydrocarbon layer [9]. Electron bombardment of this layer, the initial processing that occurs during machine comissioning, desorbs the gas layer and also results in electron-induced adsorption of carbon from carbon-containing residual-gas molecules. Water desorption and carbon deposition, amongst other processes discussed later in this paper, serve to reduce the peak SEY to near one (Figure 5, graph). This yield is close to the in-situ as-deposited TiN value [4]. The conditioning time can be reduced by glow discharge cleaning (GDC) of the chamber walls after machine assembly. Such ion sputter-removal of surface gas is much more efficient than photon/electron bombardment. Measurements of the SEY following simulated conditioning and GDC are included below.

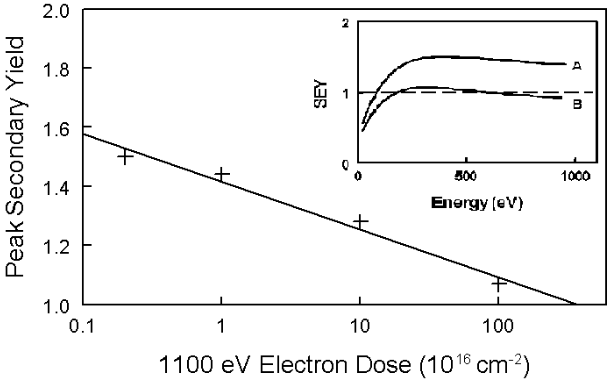

Figure 5. Peak SEY of TiN-coated Al alloy as a function of normal incidence electron beam bombardment exposure. The inset shows the complete yield curve for the first (A) and last (B) points. The data begins with a room atmosphere-exposed surface.

3.2 TiN-Coated LER Chamber Material

Angular SEY measurements were made on TiN-coated LER Al alloy coupons. The depth of the extrusion surface grooves necessitated separate measurements for glancing incidence primary electron beam both parallel and perpendicular to these grooves. These two cases are shown in Figures 6 and 7.

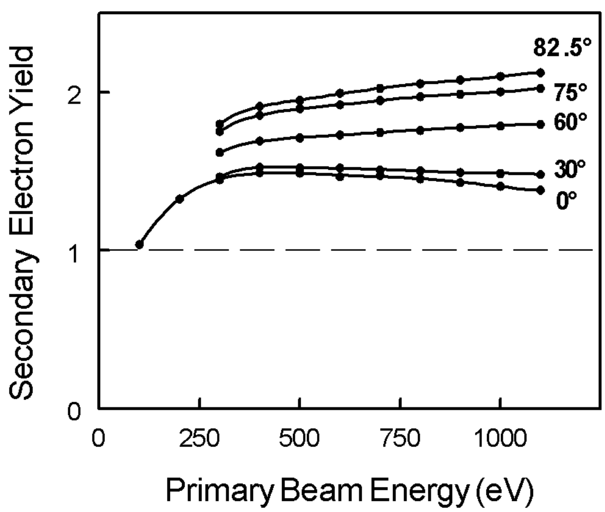

Figure 6. SEY of TiN-coated LER coupon, prior to electron dosing. Grazing incidence (82.5^{o}) electron beam is parallel to extrusion grooves.

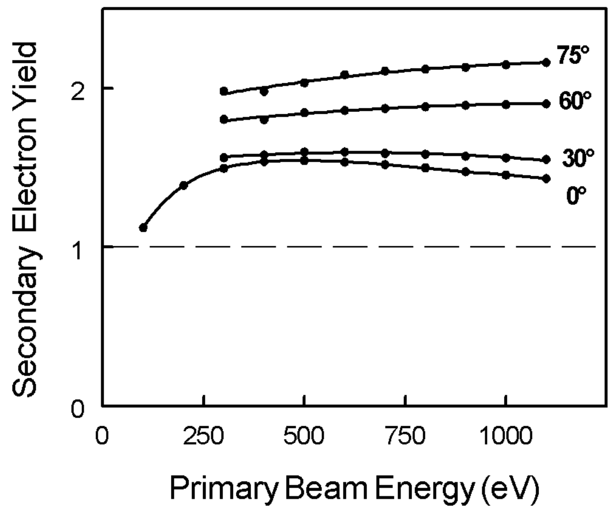

Figure 7. SEY of TiN-coated Al alloy, prior to electron dosing. Grazing incidence (75^{o}) electron beam is perpendicular to extrusion grooves.

Samples were measured multiple times at different points on the surface, to ensure consistency. Alignment of the electron beam incidence point was made at grazing incidence using the electron gun in scanning electron microscope mode and then the sample was moved slightly to an unbombarded area prior to SEY data-taking. Perpendicular-groove data could not be extended to 82.5° because of surface roughness; such data was not reliably reproducible.

Figures 6 and 7 are the atmosphere-exposed "SEY worst case" of beam chamber wall material. Electron bombardment conditioning reduces the yield, as shown in Figures 8 and 9, for the same surfaces after a normal incidence dose of approximately 10^{18} electrons-cm^{-2}.

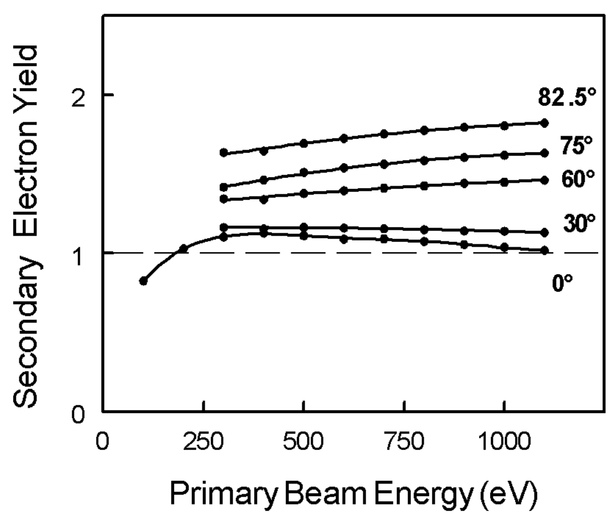

Figure 8. SEY of TiN-coated Al alloy, after electron dosing of 1.2×10^{18} electrons-cm^{-2}. Grazing incidence electron is beam parallel to extrusion grooves.

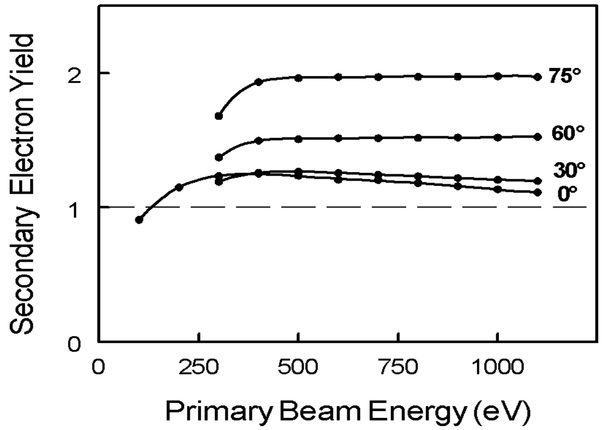

Figure 9. SEY of TiN-coated Al alloy, after electron dosing of 0.8×10^{18} electrons cm^{-2}. Grazing incidence electron is beam perpendicular to extrusion grooves.

3.3 HER Copper

Yield data for atmosphere-exposed PEP-II HER chamber material is presented in Figures 10-11.

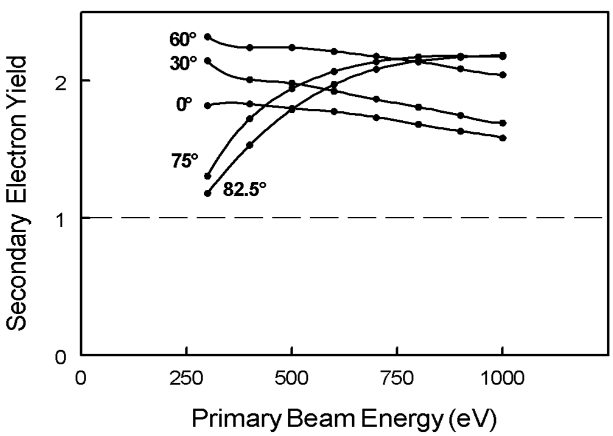

Figure 10. SEY of HER copper extrusion material, prior to electron dosing.

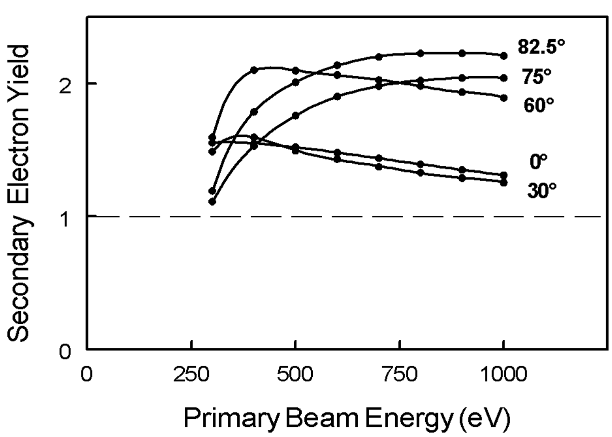

Figure 11. SEY of HER copper extrusion material, after electron dosing of 4.0×10^{18} electrons cm^{-2}.

These angular yields do not show the smooth increasing value with increasing angle of incidence demonstrated for LER alloy but were, nevertheless, experimentally repeatable. Surface finish could be a factor but the SEY data for mechanically polished and degreased OFE class one copper is similar, shown in Figure 12.

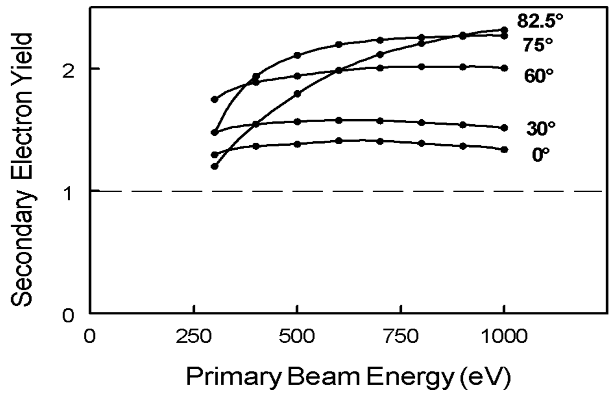

Figure 12. SEY of mechanically polished and degreased copper, for w-band acceleration applications.

Another possible cause for the results of Figure 10-11 is surface chemistry. To test this hypothesis, the HER material measured in Figures 10-11 was subsequently Ar-ion sputtered to remove any surface oxide and adventitious carbon (carbon-containing species that are adsorbed during atmospheric exposure), simulating the glow discharge cleaning (GDC) process done on the actual HER beam chambers. It was not possible to duplicate the low energy (340 eV) and high ion current of GDC using the available ion gun, so the sputtering rate instead was duplicated by using higher energy (3 keV) at lower ion current. The yields measured after this ion processing (Figure 13) are more regular, suggesting that the data of Figures 10-12 are, indeed, due to surface chemistry.

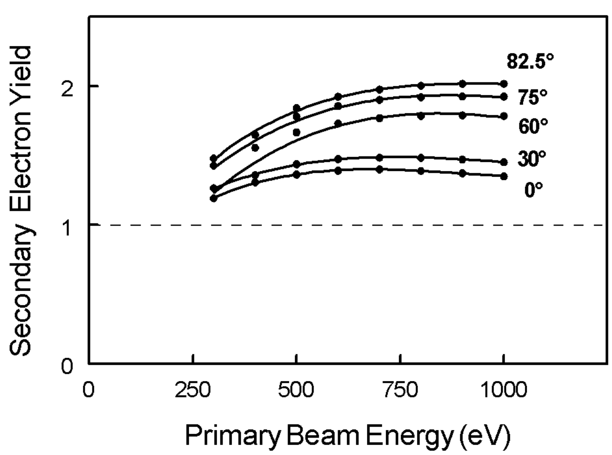

Figure 13 . SEY of Ar ion-sputtered HER copper. Ion dose parameters: 3 keV, 1.2×10^{18} ions-cm^{-2}. GDC equivalent: 0.34 keV, 2×10^{19} ions-cm^{-2}.

Some clues as to the cause of the anomaly are visible in Figure 10, namely: 1) The SEY at 300 eV, for 0^o, 30^o and 60^o appears too large, 2) the SEY at grazing incidence at 300 eV appears too low and, 3) the SEY at 1000 eV is just about right (including the increase of the SEY with angle, from normal to grazing). The data was collected from low to high primary energy at each incidence angle.

Continuing, we detail some oxidation properties of polycrystalline copper. Room temperature ambient atmospheric oxidation of clean copper results in a 2 nm terminal thickness of semiconducting cuprous oxide, Cu_2O [10]. In addition we have detected, by XPS, a smaller amount of cupric hydroxide, $Cu(OH)_2$, probably on top of the Cu_2O. The primary electron beam range at 675 eV (normal incidence *peak yield* primary energy, per Figure 13) is, by Monte Carlo simulation, ~3.0 nm in Cu_2O.

Using the above information, we present the following theory. The surface, after room air exposure, is covered with 2 nm of Cu_2O and an outer skin of $Cu(OH)_2$. This double-layer (DL) has a higher SEY than metallic copper but is extremely thin and easily electron-damaged. As a SEY measurement is begun at normal incidence, the primary beam is confined to the DL for primary energy < 675 eV. The yield is initially high but the DL is quickly damaged and drops in SEY. This effect is seen in the first few points of Figure 10, where the yield should be rising but instead is level at 0^o incidence (and actually dropping in the case of 30^o and 60^o). Still at normal incidence, the yield continues to drop from damage with increasing primary energy until 675 eV when the primary beam penetrates into the copper metal, at which point the yield becomes a combination of semiconductor and metal, causing the SEY slope to become abruptly more negative with increasing primary energy. This slope change is clearly seen in Figure 10 for 0^o, 30^o and 60^o incidence. When the primary energy is still larger, at 1000 eV, the beam is generating most of its secondaries in the metal and the SEY looks more like Figure 13. Graphically, the process is equivalent to, for example, modulating the 60^o curve of Figure 13 by an exponential decay (the "conditioning" behavior of Figure 5), and getting the result of the 60^o curve of Figure 10. This simulation is shown in Figure 14.

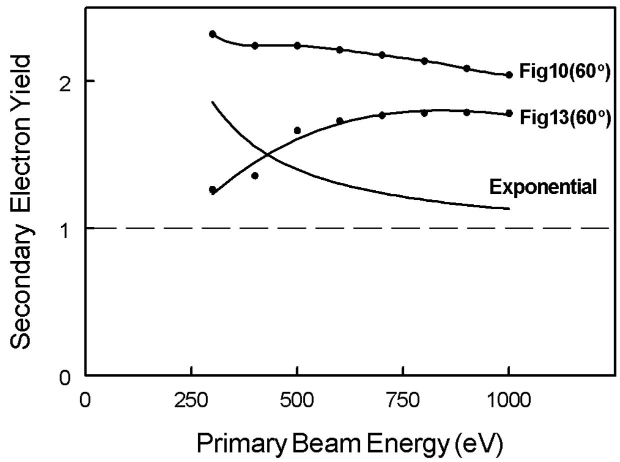

Figure 14. Graphical demonstration showing how the SEY of Figure 10,60^o might be a product of a clean copper SEY (Figure 13,60^o) convolved with a "conditioning" exponential decay, where the horizontal axis (not shown) for the decay curve is electron beam-exposure dose.

Finally, we turn to the grazing angles, 75^o and 82.5^o, in Figure 10. Initially, at 300 eV, the dielectric DL yield become so large that surface begins to charge up significantly and deflect away the primary beam. The target current goes toward zero as the deflected electrons are lost from the sample and the SEY approaches one. A stiffer higher energy primary beam deflects less and penetrates the DL, again leading, at 1000 eV, to agreement with Figure 13. The physics of Figures 10-12 is complicated but the above explanation fits the measured XPS and SEY results.

3.4 Secondary Electron Energy Distribution

Figures 6-9 show that the SEY depends most strongly on angle of incidence and, for grazing incidence, weakly on primary energy. At normal incidence, the energy dependence is stronger. Therefore, it is useful to know the emitted energy distribution of the secondaries. Incident energies around the peak of the yield, 200-600 eV, contribute most to generating secondaries at normal incidence.

The secondary electron energy distribution was measured on TiN-coated LER coupons in the SEY-measurement system, using the Auger analyzer. The analyzer acceptance slit geometry is an annulus, centered at 42° with respect to the analyzer axis and having a radial width of 6°. The results are corrected for energy-dependant analyzer transmission and plotted in Figure 15 for normal incidence primary electron beam.

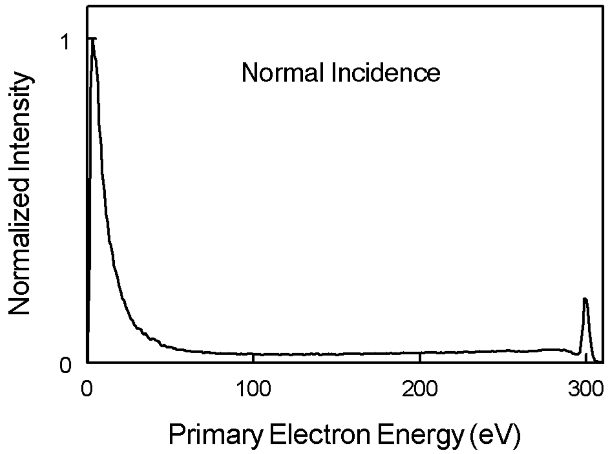

Figure 15. Collected electron energy distribution from TiN-coated Al alloy. The primary beam and analyzer axis were normal to the sample surface. The most probable secondary electron energy is 2.9 eV (8.4 eV FWHM).

The generated electron distribution curve (EDC) consists of true secondary, inelastic and elastically-reflected electrons. Forty eV is usually considered the high energy-pass cutoff for "true" secondary electrons. Relatively few primary electrons are backscattered elastically. The remainder of the generated spectrum consists of re-diffused primaries that have suffered loss events (ionizations, Augers, plasmons, etc.). The relative proportion of each kind of generated species is shown in Table I. An incidence energy of 300 eV was chosen because that is about the peak of the SEY and, hence, the most efficient for total secondary electron production. At lower primary energies, a progressively larger fraction of the distribution will be elastic [11]. The emitted electron angular spectrum will be cosine but peaked for backscattered elastics.

θ	0–40 eV	40–295 eV	295–310 eV
0°	58.9 %	36.6 %	4.5 %
82.5°	56.8 %	38.9 %	4.3 %

Table I. Normalized EDC intensity areas at normal (0°) and grazing (82.5°) primary electron incidence angle θ.

At a grazing incidence of 82.5°, the EDC still looks very similar to Figure 15 but now with the most probable energy at 2.7 eV (7.1 eV FWHM). Unlike normal incidence, more primaries will stay within the escape depth of generated low-energy secondaries, i.e., grazing incidence increases the SEY. Unfortunately, the energy analyzer has its axis along the primary beam direction, resulting in an off-sample-normal collection slit. The relative proportion of each kind of generated species is about the same (Table I), however, suggesting that the TiN surface roughness is sufficient to homogenize the secondary emission over all incidence angles.

3.5 The Secondary Yield Of Other Materials

The SEY of some materials used for beam vacuum chamber construction (and graphite, for reference) are plotted in Figure 16. The surfaces were Ar-sputtered (~$1x10^{17}$ ions-cm^{-2}) to remove most, but not all, surface contamination, as determined by Auger electron spectroscopy. Remaining carbon levels were in the 1-5 atomic per cent range. The yields of Figure 16 are those expected for beam vacuum chambers that have been glow-discharge cleaned after assembly and pumpdown.

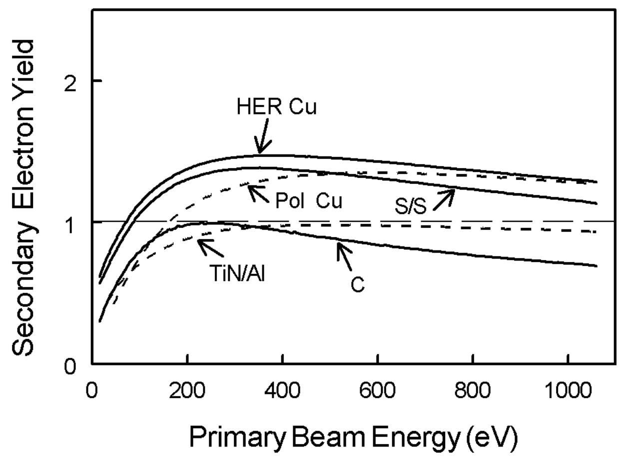

Figure 16. SEY of some materials used in accelerator/storage ring construction. Graphitic carbon is included as a measurement reference.

The yield of sputter-cleaned TiN is consistent with previous work for as-deposited, not exposed to air, films [4]. The result for polished copper ("Pol Cu") shows a shift of the peak SEY to higher primary energy, probably due to less electron-scattering (SEY-lowering) surface disorder.

4. Discussion

4.1 Primary Angle Dependence of SEY Peak Yield

SEY theory predicts that the normalized yield δ/δ_0, where δ_0 is the SEY maximum at normal incidence, should vary as 1/cos θ [12]. Figures 17 and 18 show that the experimental data from TiN/Al or Cu do not match theory for the simple case, $E_P = E_{MAX}$, (i.e., the yield is not tending toward large values as θ approaches grazing angles) and, incidentally, appears independent of conditioning (Figure 17) as well. E_P is the primary electron energy and E_{MAX} is the primary electron energy corresponding to the maximum SEY, δ_0, at normal incidence.

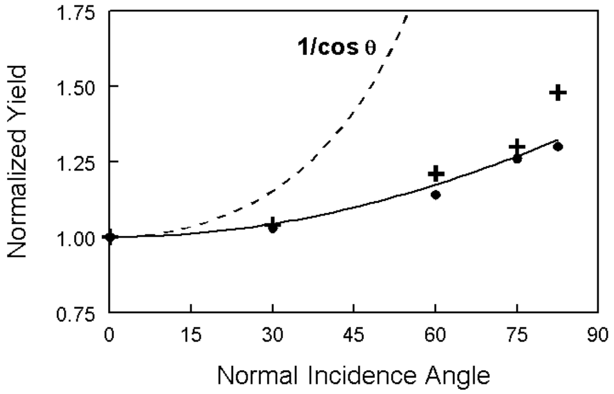

Figure 17. Normalized peak yields from TiN/Al (Figures 6 (●) and 8 (✦)) vs. primary beam incidence angle, at E_{MAX} =440 and 389 eV, respectively. The curve fit is exp [0.32 (1-cos θ)].

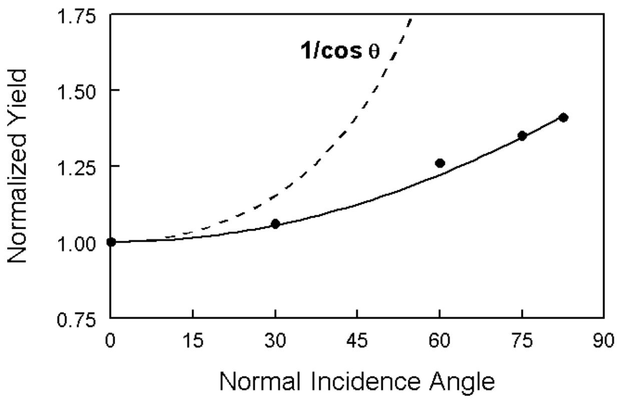

Figure 18. Normalized peak yields from HER copper (Figure 13) vs. primary beam incidence angle, at E_{MAX} =675 eV. The curve fit is exp [0.40 (1-cos θ)].

The lack of agreement with theory begins to occur far from grazing incidence, so this does not appear to be a surface-only related phenomenon. In fact, the surface finishes of the TiN/Al and Cu are quite different. However, as the primary beam angle moves toward grazing incidence, an ever-increasing fraction of primaries will exit the surface, in the forward direction, before losing their full energy to secondary electron production [13]. A simple phenomenological explanation, due to Bruining [14], accounts for the exponential dependance of Figures 17 and 18. Suppose X_m is the average depth (Figure 19) at which N_s secondary electrons are generated at normal primary beam incidence.

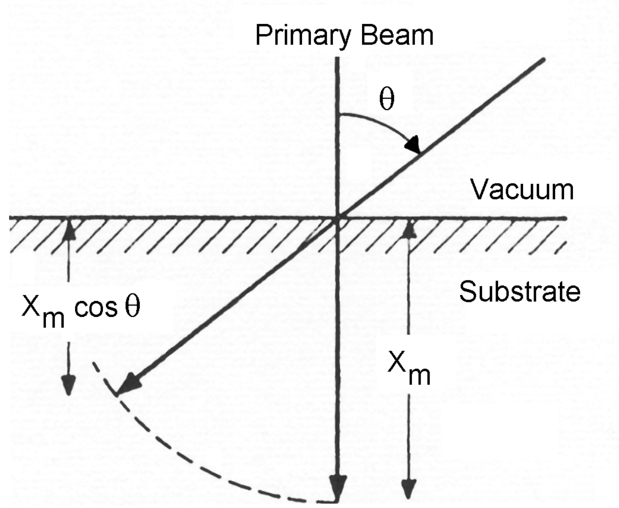

Figure 19. Schematic diagram [14] showing the secondary electron generation depth, X_m, as a function of primary electron incidence angle, θ.

Then the escape probability depends on secondary electron absorption α, and the SEY is given by

1) $\delta_0 = N_s\, e^{-\alpha X_m}$

At other than normal incidence, the yield is

2) $\delta_\theta = N_s\, e^{-(\alpha X_m \cos\theta)}$

Combining, the normalized yield as a function of primary incidence angle is given by

3) $\delta_\theta / \delta_0 = e^{\alpha X_m (1-\cos\theta)}$

which dependence fits the experimental data very well, as shown in Figures 17 and 18.

4.2 Electron Conditioning - LER

Figure 20 shows the air-exposed TiN-coated Al peak yields, as a function of electron dose, for three different samples, all pre-exposed to ambient atmosphere. The dosing and SEY measuring beams were normal to the surface. As an aside, others [15] have made such measurements to higher dose and shown that the peak yield levels off at approximately 1×10^{18} electrons cm^{-2}.

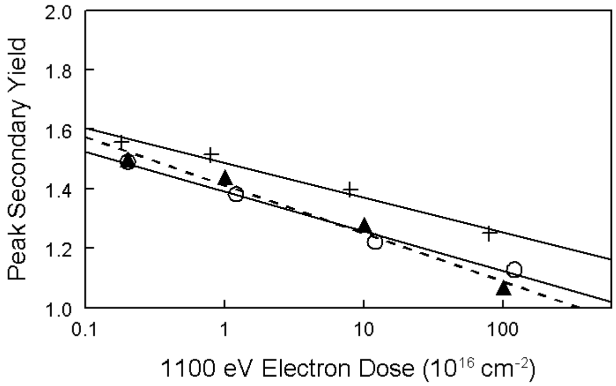

Figure 20. Peak SEY as a function of electron dose for two TiN-coated Al alloy extrusions (+,O) and TiN-coated Al sheet (▲dashed line).

The dependence of the SEY on electron dose is similar in functional form to electron-stimulated gas desorption (ESD) yields from gas-covered surfaces [11] and, because desorption of gas from the surface during conditioning results in a SEY reduction, we adopt the same formalism where the total gas desorption cross section is replaced by a "conditioning cross section." For later comparison, neutral gas ESD cross sections are on the order of 10^{-18} cm^2 with ESD ion cross sections smaller by a factor of 10-1000 [11].

Functionally, the conditioning cross section σ for Figure 20 can be calculated from the data via the first-order rate equation

$$4) \quad \delta = \delta_0 \exp(-D\,\sigma / q)$$

where δ_0 is the SEY prior to bombardment, D is the dose in coul-cm^{-2}, σ is the cross section in cm^2, and q is the electronic charge in coulombs. From Figure 20, σ is 3-4 x 10^{-19}cm^2 . This value is in the middle of the ESD cross section range.

For baked-out or GDC Al extrusion, Ding and Williams [16] measured a σ of 10^{-17}cm^2 using a much higher current density. Our lower value possibly represents a less gassy surface (the first gas layer is typically more tightly-bound then succeeding layers). Alternatively, our result may have a different SEY reduction mechanism. In particular, similar cross sections have been observed on oxidized niobium surfaces in a very clean system [4]. In that case, the production of Nb metallic suboxides was proposed as a mechanism for enhanced secondary electron-electron scattering with a concommitant reduction in the SEY.

Specifically, a list of causes for electron-induced SEY reduction must include:

1) Thermal desorption of high-SEY gases. This seems an unlikely cause because the beam power is generally too low to raise the surface temperature significantly;
2) Electron-induced surface reactions including dissociation of carbon-containing gases to elemental surface carbon, conversion of hydrocarbons to polymerized carbon, and ESD of water and gases. All of these are possible depending on initial conditions. For example, in most unbaked systems, hydrocarbons, CO and CO2 are common gas phase and surface constituents. Electron-dissociation of these have been documented on various surfaces [16,17]. Halbritter [9] has calculated that both adsorbed hydrocarbons and water lower the surface barrier to secondary electron escape (raising the yield) while elemental/polymerized carbon raises it (lowering the yield).
3) Electron-reduction of high-yield oxides. This is probably the dominant mechanism under clean surface and gas-phase conditions, for oxides and oxidized surfaces. For example, careful studies on TiO_2 [18] demonstrated that electron impact was able to displace oxygen anions, creating defects and causing electron scattering. Exposing TiN to air converts some of the TiN to TiO_2. Bombarding the TiO_2 reduces it to the titanium suboxides. Suboxides of many metals are metallic in their electronic structure thereby contributing free electrons to SEY-lowering scattering. We invoked the oxide damage picture in our discussion above of the HER angular data.
4) Electron-activated grain boundary diffusion of carbon. This phenomenon was observed on native oxide-covered aluminum [19] and niobium [20] surfaces. The primary electron beam, at energies as low as 100 eV, promotes carbon monoxide up the grain boundaries to the surface, where it is dissociated to carbon, particularly efficiently in the presence of adsorbed hydrogen. The accumulating surface carbon then results in a SEY reduction under the bombardng electron beam. Like 3) above, this mechanism is possible in clean vacuum systems.

Some combination of all of these causes probably contributes to the final result, although gas phase carbon deposition dominates in technical systems [21] and oxide-breaking in clean systems.

4.3 Electron Conditioning – HER

The air-exposed non-GDC HER copper conditioning cross-section σ is significantly smaller (4.6 x 10^{-20}cm^2, from Figure 21) than that for TiN-coated Al. The HER extrusion is smoother as noted in the material description section and, as a result, is less porous and gassy with any remaining gas tightly bound.

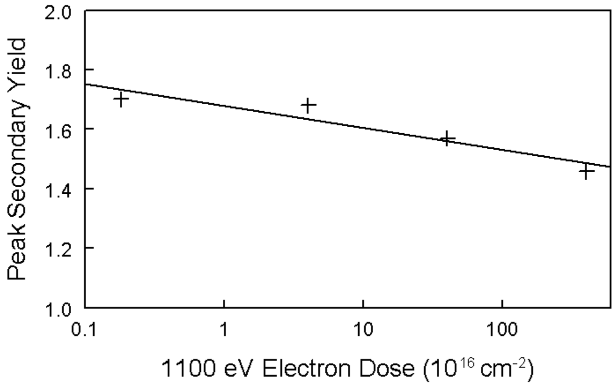

Figure 21. Peak SEY as a function of normal incidence electron dose for HER copper extrusion.

5. Conclusion

5.1 Primary Electron Angular Dependence

The data of Figures 17 and 18 for the normalized peak yields from TiN/Al and Cu are fit by almost identical functions, independent of material type, surface processing and finish. Therefore, the SEY at grazing incidence need not be known specifically at grazing angles, only the SEY at nomal incidence (preferably in the conditioned state). That number can be used to predict behavior at other angles, in the final system after in-situ conditioning.

The measurements presented here, although done on technical surfaces, are made on <u>clean</u> technical surfaces. Most accelerator/storage ring systems will, over time, be exposed to contaminants and acquire a coating of polymerized carbon which will reduce the yield substantially below that of a clean native surface. That is not to say that carbon should be introduced deliberately, because of other deleterious effects such as photodesorption of carbon-containing gases created on the surface with adsorbed water, carbon and light [22]. It would also be prudent to minimize thick oxide formation on the beam chamber surfaces to avoid a strong oxide-enhanced SEY increase at grazing angles.

5.2 Conditioning

Conditioning reduces the SEY by removing surface barrier-lowering adsorbed gases, converting surface high-SEY oxides to scatter-enhancing suboxides, and depositing low-SEY carbon species. The mix of these depends on the initial state of the surface and vacuum system. Even in systems which are bakeable to elevated temperature (> 200 ^{o}C), it is advantageous to remove the surface oxide by GDC. Some conditioning is unavoidable but shortened by GDC pre-treatment and only a modest water-removal bake (120 ^{o}C) after beamline assembly and pumdown is required.

6. Acknowledgements

The authors thank Drs. M. Furman and M. Pivi, LBL, and Prof. E. L. Garwin, SLAC, for valuable reading of the manuscript. HER samples were provided by D. Bostic, SLAC, and LER samples by K. Kennedy, LBL.

7. REFERENCES

[1] M. Izawa, Y. Sato and T. Toyomasu, Phys. Rev. Lett. **74**, 5044 (1995).
[2] K. Ohmi, Phys. Rev. Lett. **75**, 1526 (1995).
[3] E.W. Hoyt and W.P. Schulz, SLAC Technical Note **75-3**, March, 1975.
[4] E.L. Garwin, F.K. King, R.E. Kirby and O. Aita, J. Appl. Phys. **61**, 1145 (1987).
[5] K. Kennedy, M. Benapfl, B. Harteneck, F. King, R. Kirby and G. Millos, **Proc. PAC97**, Vancouver, B.C., May 12-16, 1997.
[6] J.A. Thornton, J. Vac. Sci. Technol. **A4**, 3059 (1986).
[7] R.E. Kirby, D. Wherry and M. Madden, J. Vac. Sci. Technol. **A11**, 2687 (1993).
[8] E. Hoyt, M. Hoyt, R.E. Kirby, C. Perkins, D. Wright and A. Farvid, SLAC PUB **95-6990** (1995).
[9] J. Halbritter, J. de Physique **45**, C2 (1984).
[10] T. L. Barr, J. Physical Chem. **82**, 1801 (1978).
[11] P. Redhead and J.P. Hobson and E.V. Kornelsen, **The Physical Basis of Ultrahigh Vacuum**, Chapman and Hall, Ltd. (1968), p. 140.
[12] H. Seiler, J. Appl. Phys. **54**, R1 (1983).
[13] Z.J. Ding, H. Yoshikawa, and R. Shimizu, Phys. Stat. Sol. **B161**, 257 (1990).
[14] H. Bruining, **Physics and Applications of Secondary Electron Emission**, Pergamon Press (1954).
[15] V. Baglin, B. Henrist, N. Hilleret, E. Mercier, and C. Scheuerlein, Proc. Chamonix 10, CERN-SL-2000-007 D1, Chamonix, Fr. January, 2000.
[16] M.Q. Ding and E.M. Williams, Vacuum **39**, 463 (1989).
[17] E.C. Ekwelundu and A. Ignatiev, J. Vac. Sci. Technol. **A6**, 51 (1988).
[18] R. Patel, Q. Guo, I. Cocks, E.M. Williams, E. Roman, and J.L. de Segovia, J. Vac. Sci. Technol. A15, 2553 (1997).
[19] E.L. Garwin, E.W. Hoyt, M. Rabinowitz and J. Jurow, Proc. of the 4th Int. Vacuum Congress (Manchester, 1968), Inst. of Physics and Physical Society, Pt. 1, p. 131-6 (1968).
[20] E.L. Garwin, R.E. Kirby, E.W. Hoyt and T. Momose, abstract in Vacuum 31, 597 (1981), SLAC Pub. 2716 (1981).
[21] M. Pivi, **Beam-Induced Electron Multipacting in the CERN Large Hadron Collider Accelerator LHC**, Ph.D. thesis, University of Torino (2000).
[22] P.C. Marin, Nucl. Instr. And Meth. **B89**, 69 (1994).